INTERNATIONAL JOURNAL FOR NUMERICAL METHODS IN FLUIDS, VOL. 21, 549–570 (1995)

THE USE OF A REFORMULATION OF THE HYDROSTATIC APPROXIMATION NAVIER–STOKES EQUATIONS FOR GEOPHYSICAL FLUID PROBLEMS

E. A. H. ZUUR

PROSPER, University of Neuchâtel, Rue Emile Argand 11, CH-2000 Neuchâtel, Switzerland

SUMMARY

In order to simulate geophysical general circulation processes, to simplify the governing equations of motion, often the vertical momentum equation of the Navier–Stokes equations is replaced by the hydrostatic approximation equation. The resulting equations are reformulated and a variational formulation of the linearized problem is derived. Iteration schemes are presented to solve this problem. A finite element method is discussed, as well as a finite difference method which is based on a grid that is often used in geophysical general circulation models. The schemes are extended to the non-linear case. Numerical examples are presented to demonstrate the performance of the derived iteration schemes.

KEY WORDS: incompressible Navier–Stokes equations; hydrostatic approximation; variational formulation; numerical method

1. INTRODUCTION

In order to simulate geophysical general circulation processes, to simplify the governing equations of motion, often the vertical momentum equation of the Navier–Stokes equations is replaced by the hydrostatic approximation equation. By applying the hydrostatic approximation, the prognostic feature and the highest-order spatial derivatives of the vertical velocity component are eliminated from the vertical momentum equation, which, among other things, must result in an adjustument of the boundary conditions for this velocity component. From a practical point of view the hydrostatic approximatioin is necessary when the aspect ratio, i.e. the ratio between a characteristic depth scale and a horizontal length scale of the domain, is small; without it, a strongly anisotropic elliptic operator would remain in the formulation and the assosicated discrete problem would be too ill-conditioned to apply iterative methods to find a solution.

In view of the necessity to solve three-dimensional general circulation problems in oceans or large lakes, fast algorithms are needed that can provide solutions on high-resolution grids. The history and methodology of modelling the circulation of the world ocean has been reviewed by Semtner.[1] A variety of finite difference methods have been developed to solve the primitive equations for the ocean. There are two approaches that are frequently used. The first one is based on the derivation of a prognostic volume transport streamfunction of the vertically integrated flow at each time step by eliminating the surface pressure from the horizontal momentum equations.[2,3] The second approach is based on a conversion of the original set of equations into one in which the surface pressure is more directly expressed in terms of the so-called pressure Poisson equation.[4–6] A disadvantage of both approaches is that in each case boundary value problems have to be solved at every time step, for which in practice no exact boundary conditions are at hand. For the original problem, initial conditions and boundary

CCC 0271–2091/95/070549–22

Received October 1994
Revised February 1995

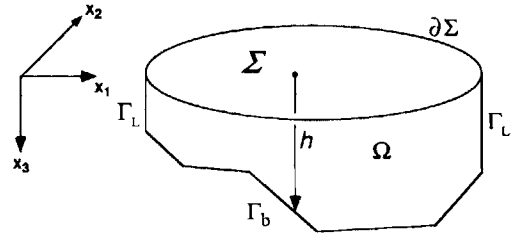

Figure 1. A 3D domain Ω with boundary $\partial\Omega = \Sigma \cup \partial\Sigma \cup \Gamma_L \cup \Gamma_b$. The function h: $\bar{\Sigma} \rightarrow \mathbb{R}$ specifies the form of the bottom Γ_b. A left-handed Cartesian system is used with the x_3-axis pointing downwards

conditions are provided only for the velocity components, so that boundary conditions for other physical quantities must be derived from these and the actual status of the flow field.

A numerical procedure is presented whereby the governing equations of motion for the ocean can be solved. No boundary conditions for physical quantities other than the velocity components are introduced. The hydrostatic approximation is fundamental to the presented approach. Further, the Boussinesq approximation, i.e. density variations are only accounted for in the buoyancy term and in the equation of state, and the rigid lid approximation, i.e. the surface of the domain is covered by a rigid lid eliminating free surface waves, are used as well.[7,8] For convenience the formulation is given with respect to a Euclidean frame of reference and the Coriolis acceleration is accounted for by using the β-approximation.[7] First the continuity equations are reformulated. The reformulation is essentially the same as that presented by Lions *et al.*[9] Then the numerical procedure is discussed. It is based on a variational formulation of the reformulated governing linearized continuity equations. This weak formulation can be solved by applying well-known techniques. Two types of spatial discretization are discussed: a finite element method and a finite difference method which is based on a grid that is often used in geophysical fluid problems. For the linearized equations the convergence of the derived iteration schemes is proven. The application of the schemes is extended to the non-linear problem. Numerical examples are presented to demonstrate the performance of the procedure.

2. THE CONTINUITY EQUATIONS

Throughout this paper a left-handed Cartesian frame of reference will be used in which the x_1 and the x_2-axis are directed horizontally and the x_3-axis is pointing downwards. A bounded domain Ω is defined in $\mathbb{R}^3$. The domain Ω is an open set in $\mathbb{R}^3$ and its boundary consists of a horizontal surface Σ, a lateral boundary Γ_L and a bottom Γ_b. The surface Σ is a regular bounded open subset in $\mathbb{R}^2$ of class C^1, say in the x_1x_2-plane at $x_3 = 0$. The bottom Γ_b is defined by the function $h \in C^1(\bar{\Sigma})$ (piecewise), which specifies the depth of the basin at each point in $\bar{\Sigma}$. It is assumed that $0 < h \leq h_{\max}$ for all points in $\bar{\Sigma}$. Σ is connected with Γ_b by a lateral boundary Γ_L (see Figure 1). It is remarked that what follows in the rest of the paper essentially applies to more general domains, but that for convenience and in view of the field of application a domain with a flat horizontal surface is used.

We are interested in motions on a geophysical scale and the effect of the use of a non-inertial frame of reference which is attached to the rotating earth is included by the β-approximation of the Coriolis acceleration,[7] with Coriolis factor $\chi \in C^0(\bar{\Omega})$. The Boussinesq approximation and the rigid lid approximation are used as well.[8] Turbulent viscosity in the horizontal and vertical directions is represented by constant turbulent viscosity coefficients A_H and A_V respectively, i.e. by Reynolds stresses.

Large-scale geophysical motion occurs within a thin sheet of fluid and this gives a disparity between horizontal and vertical scales. The influence of this disparity becomes evident by writing the governing

equations in a non-dimensional form. Therefore let L be a characteristic horizontal length, D be a vertical one and U be a characteristic scale for the horizontal velocity. The aspect ratio is defined by $\delta = D/L$ and it may be assumed throughout that $\delta \ll 1$. Further, let u_i be the velocity component in the i-direction ($i = 1, 2, 3$). With the mass conservation equation and the Boussinesq approximation we have

$$\frac{\partial u_1}{\partial x_1} + \frac{\partial u_2}{\partial x_2} + \frac{\partial u_3}{\partial x_3} = 0, \tag{1}$$

and it follows immediately that we must have $u_3 = O(\delta U)$. The non-dimensional Rossby number and the horizontal and vertical Ekman numbers are defined respectively as

$$r = \frac{U}{\chi_{\max} L}, \qquad E_H = 2\frac{A_H}{\chi_{\max} L^2}, \qquad E_V = 2\frac{A_V}{\chi_{\max} D^2}, \tag{2}$$

where $\chi_{\max}$ may be taken as the maximum Coriolis factor in absolute value in Ω, i.e. the factor at maximum/minimum latitude. There is much uncertainty associated with the values of the turbulent viscosity coefficients A_H and A_V and estimates in the ocean or large lakes vary enormously. It is not unreasonable, however, to assume that the turbulent viscosity is to some extent proportional to the square of the associated length scale. At least this would mean that E_H and E_V have the same order of magnitude. Merely for convenience in order to keep the expressions that follow simple, we will take $E_H = E_V = 2\mu$. With the above definitions the Navier–Stokes equations in non-dimensional form are written as[7]

$$\begin{aligned}
&r\left(\frac{\partial u_1}{\partial t} + u_1\frac{\partial u_1}{\partial x_1} + u_2\frac{\partial u_1}{\partial x_2} + u_3\frac{\partial u_1}{\partial x_3}\right) - \chi u_2 - \mu\left(\frac{\partial^2 u_1}{\partial x_1^2} + \frac{\partial^2 u_1}{\partial x_2^2} + \frac{\partial^2 u_1}{\partial x_3^2}\right) = -\frac{\partial P}{\partial x_1} + f_1,\\
&r\left(\frac{\partial u_2}{\partial t} + u_1\frac{\partial u_2}{\partial x_1} + u_2\frac{\partial u_2}{\partial x_2} + u_3\frac{\partial u_2}{\partial x_3}\right) + \chi u_1 - \mu\left(\frac{\partial^2 u_2}{\partial x_1^2} + \frac{\partial^2 u_2}{\partial x_2^2} + \frac{\partial^2 u_2}{\partial x_3^2}\right) = -\frac{\partial P}{\partial x_2} + f_2,\\
&\delta^2 r\left(\frac{\partial u_3}{\partial t} + u_1\frac{\partial u_3}{\partial x_1} + u_2\frac{\partial u_3}{\partial x_2} + u_3\frac{\partial u_3}{\partial x_3}\right) - \delta^2\mu\left(\frac{\partial^2 u_3}{\partial x_1^2} + \frac{\partial^2 u_3}{\partial x_2^2} + \frac{\partial^2 u_3}{\partial x_3^2}\right) = -\frac{\partial P}{\partial x_3} + f_3,
\end{aligned} \tag{3}$$

where u_1, u_2, u_3 and P denote the non-dimensional velocity components and pressure respectively. Body force components f_1, f_2 and f_3 have been added which will be specified later on. With the above definitions, for the non-dimensional Coriolis factor $\chi \in C^0(\bar{\Omega})$ we have $\| \chi \|_\infty \leq 1$. The magnitude of the Rossby number r gives the relative importance between the inertial forces and the Coriolis acceleration, while the magnitude of the Ekman number μ represents the relative importance between the turbulent viscous forces and the Coriolis acceleration. For general circulation problems in the ocean, typical orders of magnitude for these numbers at mid-latitude are $r = O(10^{-1})$ and $\mu = O(10^{-2})$. A typical order of magnitude for the aspect ratio is $\delta = O(10^{-3})$. The hydrostatic approximation is obtained by taking $\delta = 0$ in (3).

With $r = 0$, $\chi = 0$ and $\delta = 1$ in (3) we find the classical Stokes equations. Subject to appropriate boundary conditions, there exists a variety of iteration methods to solve the Stokes problem. An optimization method such as the Uzawa method, whose application will be discussed later on, is in principle suitable for solving a discrete form of the above equations with $\delta > 0$. However, the number of iterations to obtain an approximate solution with a prescribed precision will increase if δ is taken smaller and will tend to infinity if $\delta \to 0$. This behaviour can easily be verified in practice. We will not give a formal proof of the statement, but it will be made plausible. The elliptic operator which is acting on the velocity field (u_1, u_2, u_3) is anisotropic owing to the factor δ^2. When this operator is discretized to find a numerical solution, the eigenvalue spectrum of the resulting matrix

depends on the factors μ and $\delta^2\mu$. When δ is taken smaller, basically the spectrum will be enlarged towards zero, and when $\delta \to 0$, the operator will tend to become singular. The enlargement of the spectrum will increase the number of iterations and the method will break down if the matrix becomes singular.

This remark suggests that the equations in their present form are not an appropriate starting point to derive iteration schemes that can be applied to find solutions when the hydrostatic approximation is used. In order to overcome this problem, we shall first given an alternative form of (3) by taking the kinematic condition into account, i.e. that there is no normal flow through the surface Σ and the bottom Γ_b. By imposing this condition, an equivalence can be used that is readily established with Leibniz' integration rule:

$$\begin{aligned} &\sum_{i=1}^{3} \frac{\partial u_i}{\partial x_i} = 0 \quad \text{in } \Omega \quad \text{and} \quad \sum_{i=1}^{3} u_i n_i = 0 \quad \text{on } \Sigma \text{ and } \Gamma_b \iff \\ &\sum_{i=1}^{2} \frac{\partial}{\partial x_i} \int_0^h u_i \, dz = 0 \quad \text{on } \Sigma \quad \text{and} \quad u_3 = -\sum_{i=1}^{2} \int_0^{x_3} \frac{\partial u_i}{\partial x_i} \, dz \quad \text{in } \bar{\Omega}, \end{aligned} \tag{4}$$

where $n = (n_1, n_2, n_3)$ is the outward-pointing normal vector on Σ and Γ_b. This means that the kinematic condition and the condition that the velocity field must be divergence-free in Ω can be replaced by a condition that relates only to the horizontal components, namely that vertically integrated horizontal velocity components are divergence-free in the plane Σ, and by a relation that explicitly determines the vertical velocity component. Further, to avoid the anisotropy in the elliptic operator, the hydrostatic approximation is used by setting $\delta = 0$ in (3). Then the pressure P can be decomposed into a non-hydrostatic pressure part P_s which is independent of the vertical co-ordinate and a hydrostatic part as

$$P = P_s + \int_0^{x_3} f_3 \, dz, \quad \text{with } \frac{\partial P_s}{\partial x_3} = 0. \tag{5}$$

The non-hydrostatic pressure P_s is a consequence of the rigid lid approximation, but physically it can be interpreted as a surface elevation of the water column. By assuming sufficient regularity of the body force component f_3, the problem can be reformulated in terms of the pressure P_s by entering the given hydrostatic part into the horizontal body force components f_1 and f_2 in (3). For the moment, homogeneous Dirichlet boundary conditions are specified for the horizontal velocity components, i.e. we set $u_1 = u_2 = 0$ on $\partial\Omega$. We arrive at an equivalent formulation of (1) and (3) with $\delta = 0$. Writing henceforth P for P_s, it takes the form

$$\begin{aligned} &r\left(\frac{\partial u}{\partial t} + u_1 \frac{\partial u}{\partial x_1} + u_2 \frac{\partial u}{\partial x_2} + u_3 \frac{\partial u}{\partial x_3}\right) + \mathrm{X}u - \mu \Delta u = -\mathrm{grad}_\Sigma(P) + f, \\ &0 = \frac{\partial P}{\partial x_3}, \\ &\mathrm{div}_\Sigma\left(\int_0^h u \, dx_3\right) = 0, \\ &u = 0 \quad \text{on } \partial\Omega, \qquad u(x, 0) = u_0(x), \\ &u_3 = -\int_0^{x_3} \mathrm{div}_\Sigma(u) \, dz, \end{aligned} \tag{6}$$

where

$$u = (u_1, u_2)^{\mathrm{T}} : \Omega \times (0, T) \to \mathbb{R}^2, \qquad P : \Omega \times (0, T) \to \mathbb{R}, \qquad f = (f_1, f_2)^{\mathrm{T}} : \Omega \times (0, T) \to \mathbb{R}^2,$$

$$\Delta u = \frac{\partial^2 u}{\partial x_1^2} + \frac{\partial^2 u}{\partial x_2^2} + \frac{\partial^2 u}{\partial x_3^2}, \qquad \mathrm{grad}_\Sigma(P) = \left(\frac{\partial P}{\partial x_1}, \frac{\partial P}{\partial x_2}\right)^{\mathrm{T}},$$

$$\mathrm{div}_\Sigma\left(\int_0^h u \, \mathrm{d}x_3\right) = \frac{\partial}{\partial x_1}\int_0^h u_1 \, \mathrm{d}z + \frac{\partial}{\partial x_2}\int_0^h u_2 \, \mathrm{d}z, \qquad \mathrm{X}u = \chi \begin{pmatrix} 0 & -1 \\ 1 & 0 \end{pmatrix} \begin{pmatrix} u_1 \\ u_2 \end{pmatrix},$$

with $\chi \in C^0(\bar{\Omega})$ the Coriolis factor. The above system will be referred to as the hydrostatic approximation (hydapp) Navier–Stokes problem. When $r = 0$, we will speak of the hydapp Stokes problem (with Coriolis term). Notice that in this case the vertical velocity component has disappeared from the first equation of (6) and we are left with the problem of finding the horizontal velocity $u \in \mathbb{C}^2(\bar{\Omega})$ and the pressure $P \in C^1(\bar{\Omega})$. Once the horizontal velocity has been found, the vertical velocity component can be found explicitly. The boundary conditions for this component are indirectly imposed by the kinematic condition through (4). This means in particular that, in contrast with the full Navier–Stokes problem without the hydrostatic approximation, no boundary condition is specified on vertical sides Γ_L for this velocity component.

The above reformulation is essentially the same as that presented by Lions *et al.*[9] For a theoretical treatment of these and related non-linear systems of equations we refer to their work. In the rest of the paper we wish to arrive at fast applicable iteraction schemes to solve a discrete form of system (6). In order to do so, appropriate numerical schemes will be derived by analysing the linearized system of equations and extending the results to the non-linear case.

3. THE HYDAPP STOKES PROBLEM

3.1. A variational formulation of the hydapp Stokes problem

Let $D(\Omega)$ and $D(\Sigma)$ denote the spaces of $C^\infty(\Omega)$- and $C^\infty(\Sigma)$-functions with compact support contained in the bounded open sets Ω in $\mathbb{R}^3$ and Σ in $\mathbb{R}^2$, respectively. Let $L^2(\Omega)$ and $L^2(\Sigma)$ be the Hilbert spaces of real functions on Ω and Σ respectively, which are square integrable in the Lebesgue sense and on which the usual scalar products are defined with associated norms:

$$(\phi, \psi)_{L^2(\Omega)} = \int_\Omega \phi\psi \, \mathrm{d}\Omega, \qquad \|\phi\|_{L^2(\Omega)} = (\phi, \phi)^{1/2}_{L^2(\Omega)},$$

$$(\eta, \vartheta)_{L^2(\Sigma)} = \int_\Sigma \eta\vartheta \, \mathrm{d}\Sigma, \qquad \|\eta\|_{L^2(\Sigma)} = (\eta, \eta)^{1/2}_{L^2(\Sigma)}.$$

Further, two Sobolev spaces of order one are denoted by

$$H_0^1(\Omega) = \left\{ \phi \in L^2(\Omega) \middle| \frac{\partial \phi}{\partial x_i} \in L^2(\Omega) \; (i = 1, 2, 3), \; \gamma\phi \Big|_{\partial\Omega} = 0 \right\},$$

$$H_0^1(\Sigma) = \left\{ \eta \in L^2(\Sigma) \middle| \frac{\partial \eta}{\partial x_i} \in L^2(\Sigma) \; (i = 1, 2), \; \gamma\eta \Big|_{\partial\Sigma} = 0 \right\},$$

where γ is the trace operator; they have respective Hilbert structures given by

$$(\phi, \psi)_{H_0^1(\Omega)} = \sum_{j=1}^{3} \int_\Omega \frac{\partial \phi}{\partial x_j} \frac{\partial \psi}{\partial x_j} \, d\Omega, \qquad \|\phi\|_{H_0^1(\Omega)} = (\phi, \phi)_{H_0^1(\Omega)}^{1/2},$$

$$(\eta, \vartheta)_{H_0^1(\Sigma)} = \sum_{j=1}^{2} \int_\Sigma \frac{\partial \eta}{\partial x_j} \frac{\partial \vartheta}{\partial x_j} \, d\Sigma, \qquad \|\eta\|_{H_0^1(\Sigma)} = (\eta, \eta)_{H_0^1(\Sigma)}^{1/2}.$$

We shall often be concerned with two-dimensional vector functions with components in one of these spaces. We shall use the notation $\mathbb{L}^2(\Omega) = \{L^2(\Omega)\}^2$, $\mathbb{L}^2(\Sigma) = \{L^2(\Sigma)\}^2$, $\mathbb{H}_0^1(\Omega) = \{H_0^1(\Omega)\}^2$ and $\mathbb{H}_0^1(\Sigma) = \{H_0^1(\Sigma)\}^2$ and it is assumed that these product spaces are equipped with the usual product norms. To relate the spaces $\mathbb{H}_0^1(\Sigma)$ and $\mathbb{H}_0^1(\Sigma)$, the following result is derived.

Proposition 1

Let $h \in C^1(\bar{\Sigma})$, with $h > 0$ in $\bar{\Sigma}$, define the depth of domain Ω with surface Σ as described in Section 2. Then

$$u \to \bar{u} \overset{\text{def}}{=} \int_0^h u \, dz$$

defines a mapping from $\mathbb{H}_0^1(\Omega)$ onto $\mathbb{H}_0^1(\Sigma)$ for which

$$\|\bar{u}\|_{\mathbb{H}_0^1(\Sigma)}^2 \leq h_{\max} \|u\|_{\mathbb{H}_0^1(\Omega)}^2,$$

where $h_{\max}$ is the maximum depth of Ω.

Proof. For $u \in \mathbb{C}_0^1(\bar{\Omega})$, by using the Cauchy–Schwartz inequality and Fubini's theorem, the result readily follows. Since $\mathbb{C}_0^1(\bar{\Omega})$ is a dense subspace of $\mathbb{H}_0^1(\Omega)$ with continuous injection, the inequality can be extended to all elements of $\mathbb{H}_0^1(\Omega)$. Further, for every $\eta \in \mathbb{H}_0^1(\Sigma)$ there exists a $\phi \in \mathbb{H}_0^1(\Omega)$ with $\eta = \bar{\phi}$. For this purpose take any $\lambda \in D((0, 1))$ with $\int_0^1 \lambda(z) \, dz = 1$. Since h is a positive function in $\bar{\Sigma}$, for given $\eta \in \mathbb{H}_0^1(\Sigma)$ one may verify that

$$\phi = \eta \frac{1}{h} \lambda\left(\frac{z}{h}\right) \in \mathbb{H}_0^1(\Omega)$$

and thus $\bar{\phi} = \eta$. □

Taking $r = 0$ in (6), multiplying the equations by a test function and integrating the result over Ω using Green's theorem leads to the following variational formulation for the hydapp Stokes problem with Coriolis term:

$$\begin{cases} \text{given } f \in \mathbb{L}^2(\Omega) \\ \text{find } u \in V \quad \text{such that} \\ a(u, v) = L(v), \quad \forall v \in V, \end{cases} \tag{7}$$

where

$$a(u, v) = (Xu, v)_{\mathbb{L}_2(\Omega)} + \mu(u, v)_{\mathbb{H}_0^1(\Omega)},$$

$$L(v) = (f, v)_{\mathbb{L}_2(\Omega)},$$

$$V = \{v \in \mathbb{H}_0^1(\Omega) | \operatorname{div}_\Sigma(\bar{v}) = 0 \text{ a.e. in } \Sigma\}.$$

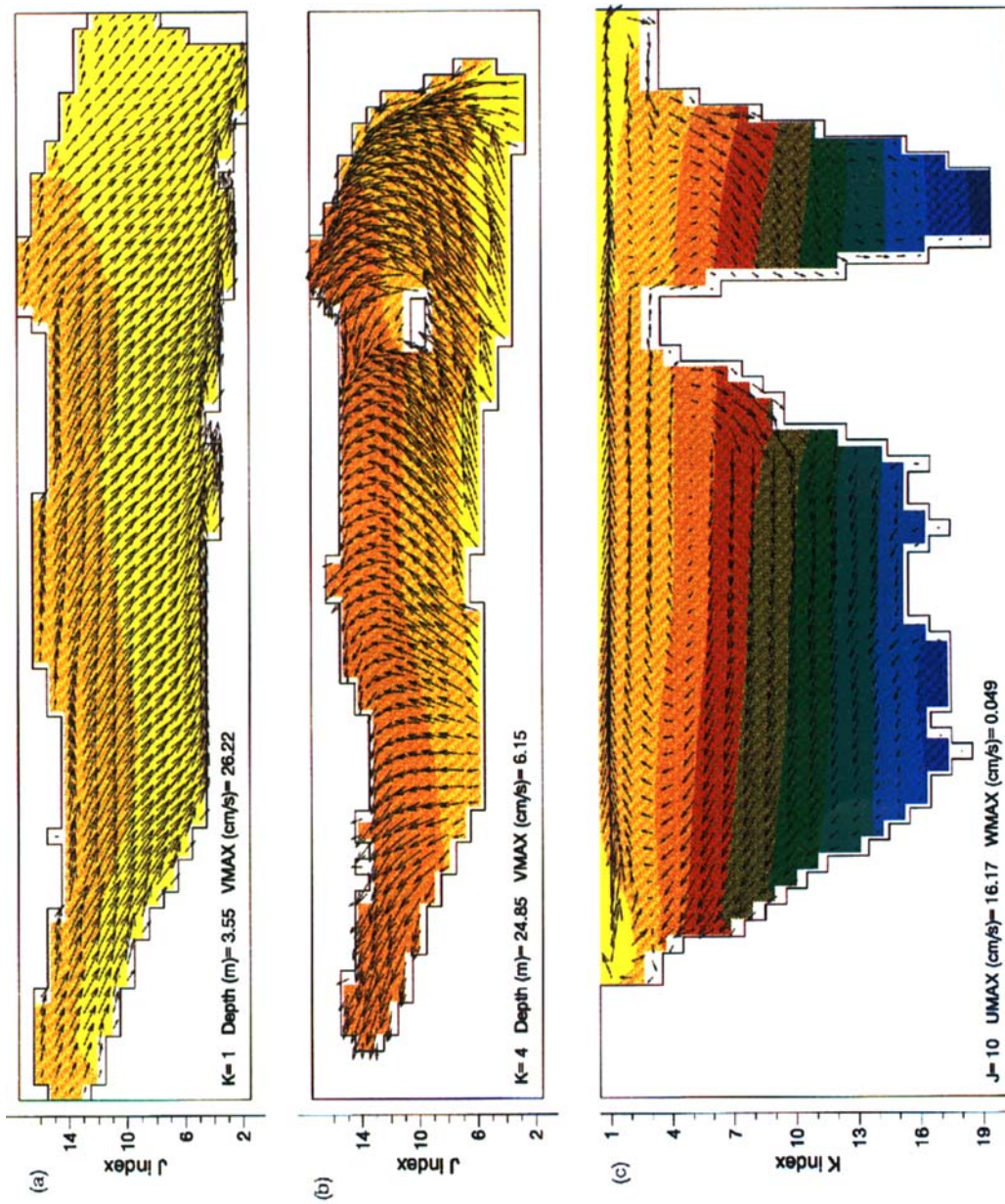

Plate 1. Temperature and velocity fields ((a,b) horizontal levels, (c) vertical slice) after 12 h wind forcing of a SW wind with constant speed 7.5 m/s. Colours refer to temperature (see plate 2). The scaling factors for velocity arrows are adjusted in each plot according to the maximum velocity that occurs at that level or slice. The magnitude of the longest arrow is denoted under the corresponding plot. The depthlevel is indicated by the *K*-value and the slice by the *J*-value (see Figure 6). The SW wind drags the surface currents eastwards, inducing upwelling in the west part and downwelling in the east part of the lake. The flux in the upper layers is balanced by a counter-current in the deeper ones

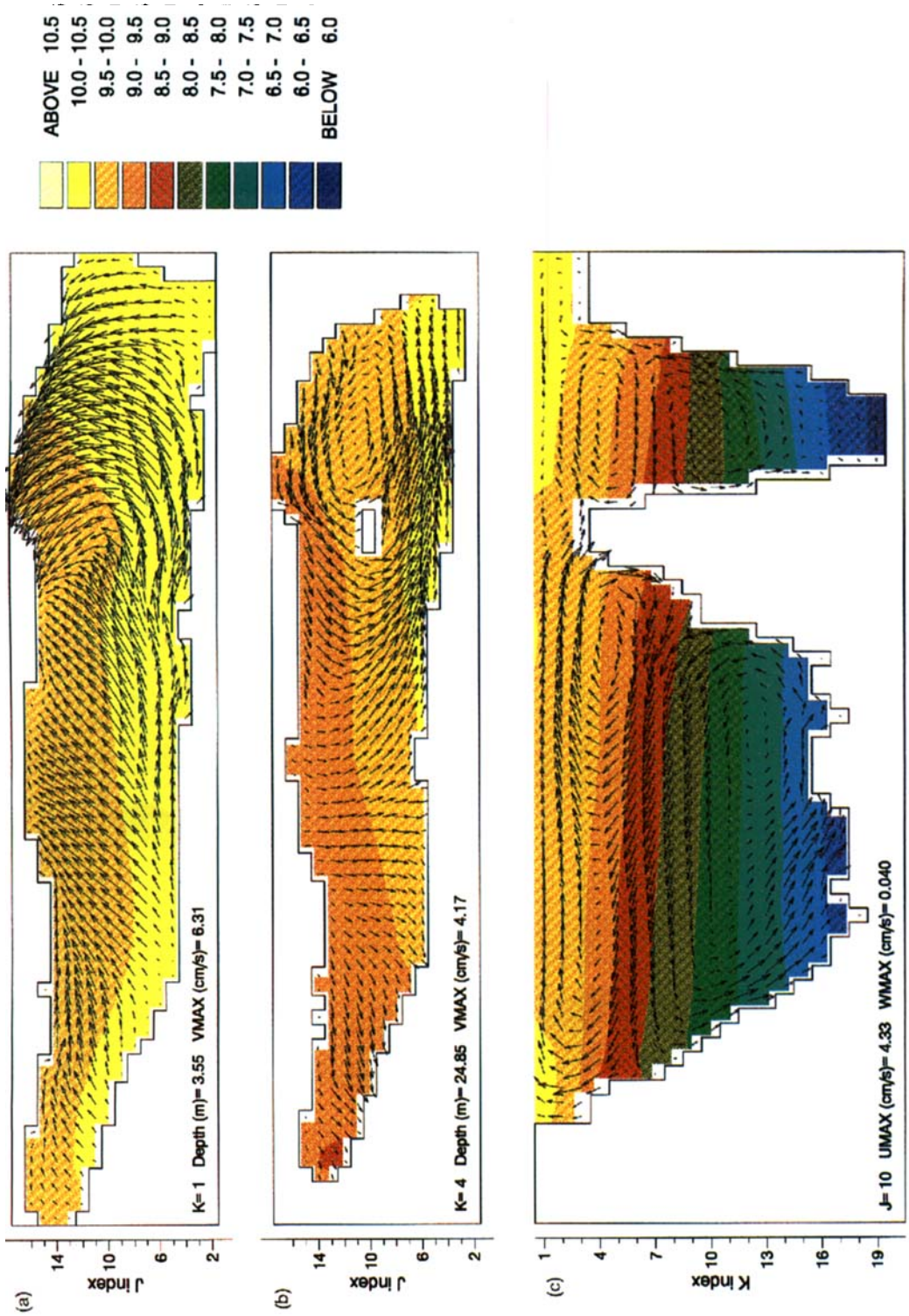

Plate 2. Temperature and velocity fields ((a,b) horizontal levels, (c) vertical slice) 12 h after the wind was turned off. In the vertical slice one may notice the subdivision into two oppositely rotating cells, epilimnetic and hypolimnetic

In deriving (7), we used

$$\int_\Omega -\text{grad}_\Sigma(P)\cdot v\,d\Omega = -\int_{\partial\Sigma} p\bar{v}\cdot n_\Sigma\,d\sigma + \int_\Sigma p\,\text{div}_\Sigma(\bar{v})\,d\Sigma = 0, \quad \forall v \in V,$$

where n_Σ is the outward-pointing normal vector on $\partial\Sigma$ and $p = p(x, y)$ is the surface pressure defined on Σ. Further, notice that $\text{div}_\Sigma(\bar{\cdot})$ is Lipschitz-continuous, because with Proposition 1 it follows that

$$\|\text{div}_\Sigma(\bar{u})\|_{L^2(\Sigma)} \leq \|\bar{u}\|_{\mathbb{H}_0^1(\Sigma)} \leq \mathscr{C}\|u\|_{\mathbb{H}_0^1(\Omega)},$$

with $\mathscr{C} = \sqrt{h_{\max}}$ the Lipschitz constant.

When the horizontal velocity is known, for the vertical velocity we get the following:

$$\begin{cases} \text{given } u \in V, \\ \text{find } u_3 \in Z \quad \text{such that} \\ \left(\dfrac{\partial u_3}{\partial x_3},\ w\right)_{L^2(\Omega)} = -(\text{div}_\Sigma(u),\ w)_{L^2(\Omega)}, \quad \forall w \in Z, \end{cases} \tag{9}$$

where

$$Z = \left\{ w \in L^2(\Omega) \middle| \frac{\partial w}{\partial x_3} \in L^2(\Omega),\ \gamma w\Big|_\Sigma = 0 \right\}.$$

The space V is separable as a closed subspace of $\mathbb{H}_0^1(\Omega)$. Further, $a(.,.)$ is a bilinear continuous form which is coercive, with coercive constant $\mu > 0$, and from the classical projection theorem it follows that (7) has a unique solution. It will be shown how this solution relates to a solution of problem (6) with $r = 0$. First we prove the following proposition.

Proposition 2

Let $h \in C^1(\bar{\Sigma})$, with $h > 0$ in $\bar{\Sigma}$, and let $Q \in H^{-1}(\Omega)$, the dual space of $\mathbb{H}_0^1(\Omega)$, with $\partial Q/\partial x_3 = 0$ a.e. in Σ. Then one may define $q \in H^{-1}(\Sigma)$ through

$$\int_\Sigma q\bar{\phi}\,d\Sigma = \int_\Omega Q\phi\,d\Omega, \quad \forall \phi \in H_0^1(\Omega).$$

(Notice that the inverse statement holds trivially: for given $q \in H^{-1}(\Sigma)$ the left-hand side defines a functional $Q \in H^{-1}(\Sigma)$ for which $\partial Q/\partial x_3 = 0$ a.e. in Ω.)

Proof. From Proposition 1 we have that $\phi \to \bar{\phi}$ defines a mapping from $H_0^1(\Omega)$ onto $H_0^1(\Sigma)$. First it is shown that the functional q is uniquely determined for every $\eta \in H_0^1(\Sigma)$ for which there exists a $\phi \in H_0^1(\Omega)$ with $\eta = \bar{\phi}$. By linearity it is sufficient to show that

$$\left(\bar{\phi} = 0 \implies \int_\Omega Q\phi\,d\Omega = 0\right), \quad \forall \phi \in H_0^1(\Omega).$$

Therefore let $\phi \in D(\Omega)$ with $\bar{\phi} = 0$ and define

$$\psi = \int_0^{x_3} \phi\,dz.$$

Then $\psi \in D(\Omega)$, because the support of ψ is contained in that of ϕ, and we get

$$\int_\Omega Q\phi \, d\Omega = \int_\Omega Q \frac{\partial \psi}{\partial x_3} \, d\Omega = -\int_\Omega \frac{\partial Q}{\partial x_3} \psi \, d\Omega = 0,$$

which result may be extended to $\psi \in H_0^1(\Omega)$, since $D(\Omega)$ is dense in $H_0^1(\Omega)$ with continuous injection. Second, as the mapping $\phi \to \bar{\phi}$ is onto, q is determined for every $\eta \in H_0^1(\Sigma)$. □

Clearly, if $u \in \mathbb{C}^2(\bar{\Omega})$ is a classical solution of problem (6) with $r = 0$, then u satisfies the weak formulation (7). Inversely, when u satisfies (7), it may be shown that $Xu - \mu\Delta u - f$ can be interpreted as a distribution in $\{D'(\Omega)\}^2$, where $D'(\Omega)$ is the dual space of $D(\Omega)$. It may be verified that for every $\phi \in \{D(\Omega)\}^2$ we have $\partial\phi/\partial x_3 \in V$, so that

$$\frac{\partial}{\partial x_3}(Xu - \mu\Delta u - f) = 0 \quad \text{in } \{D'(\Omega)\}^2. \tag{10}$$

On account of Proposition 2, $Xu - \mu\Delta u - f$ defines a functional on $\mathbb{H}_0^1(\Sigma)$ that will be denoted by $\sigma(Xu - \mu\Delta u - f)$ and for which

$$\int_\Sigma \sigma(Xu - \mu\Delta u - f) \cdot \eta \, d\Omega = 0, \quad \forall \eta \in \mathbb{H}_0^1(\Sigma), \quad \text{with } \operatorname{div}_\Sigma(\eta) = 0.$$

A theorem of de Rham[10] proves that a functional on $\mathbb{H}_0^1(\Sigma)$ which is equal to zero on divergence-free vector fields can be written as the gradient of a distribution. Thus there exists a $p \in D'(\Sigma)$ such that

$$\sigma(Xu - \mu\Delta u - f) = -\operatorname{grad}_\Sigma(p) \quad \text{in } \{D'(\Sigma)\}^2. \tag{11}$$

Notice that $p \in L^2(\Sigma)$, since all first derivatives of p are in $H^{-1}(\Sigma)$ and Σ is of class C^1.[11] Here p is defined up to an additive constant and in the rest of the paper we will take $p \in L^2(\Sigma)/\mathbb{R}$, where

$$L^2(\Sigma)/\mathbb{R} = \left\{ p \in L^2(\Sigma), \int_\Sigma p \, d\Sigma = 0 \right\}.$$

Now define $P \in D'(\Omega)$ through

$$\int_\Omega P\phi \, d\Omega = \int_\Sigma p\bar{\phi} \, d\Sigma, \quad \forall \phi \in D(\Omega). \tag{12}$$

Then with Proposition 2 and (10)–(12) we get

$$Xu - \mu\Delta u = -\operatorname{grad}_\Sigma(P) + f \quad \text{in } \{D'(\Omega)\}^2,$$

with

$$\frac{\partial P}{\partial x_3} = 0 \quad \text{in } D'(\Omega).$$

Because $u \in V$, we immediately have $\gamma u = 0$ in $\mathbb{H}^{1/2}(\partial\Omega)$. Thus a solution of (7) is also a solution in the distributional sense of problem (6) with $r = 0$.

3.2. A duality method to solve the hydapp Stokes problem

In order to find a solution of the variational formulation (7) and to avoid the use of a projection operator on V, a duality method may be used. For this purpose an optimization algorithm such as the

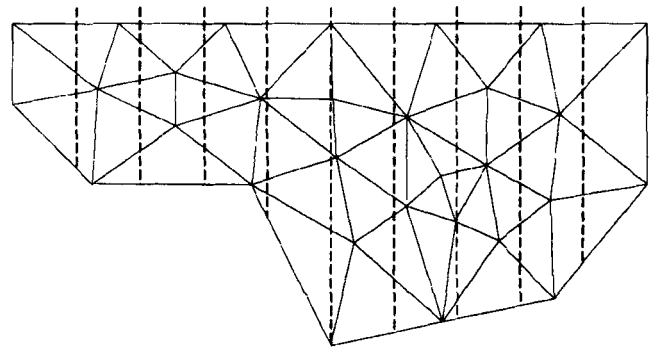

Figure 2. Subdivision of a 2D domain into finite elements for the horizontal velocity component. The surface is subdivided into 10 p-intervals

Uzawa method is suitable.[12] The algorithm is started with an arbitrary $p^0 \in L^2(\Sigma)/\mathbb{R}$. When p^m is known, u^{m+1} and p^{m+1} $(m \geq 0)$ are defined by the conditions

$$u^{m+1} \in \mathbb{H}_0^1(\Omega),$$

$$(Xu^{m+1}, v)_{\mathbb{L}^2(\Omega)} + \mu(u^{m+1}, v)_{\mathbb{H}_0^1(\Omega)} - (p^m, \operatorname{div}_\Sigma(\bar{v}))_{L^2(\Sigma)} = (f, v)_{\mathbb{L}^2(\Omega)}, \quad \forall v \in \mathbb{H}_0^1(\Omega), \tag{13}$$

$$p_{m+1} \in L^2(\Sigma),$$

$$(p^{m+1} - p^m, q)_{L^2(\Sigma)} + \alpha(\operatorname{div}_\Sigma(\overline{u^{m+1}}), q)_{L^2(\Sigma)} = 0, \quad \forall q \in L^2(\Sigma),$$

where $\alpha > 0$ is a fixed number. The existence and uniqueness of the solution u^{m+1} at each iteration follow from the projection theorem. If α satisfies

$$0 < \alpha < \frac{2\mu}{\mathscr{C}^2}, \tag{14}$$

where $\mathscr{C} = \sqrt{h_{\max}}$ is the Lipschitz constant in (8), then as $m \to \infty$, the solution $\{u^m, p^m\}$ converges to the solution $\{u, p\}$ of problem (7), with p defined as in (11), in the following sense.

$$u^m \to u \quad \text{strongly in } \mathbb{H}_0^1(\Omega),$$
$$p^m \to p \quad \text{weakly in } L^2(\Sigma)/\mathbb{R}.$$

The proof is similar to the proof of convergence of the Uzawa method for the Stokes problem (Reference 13, pp. 138–142). The principal difference lies in the different constraints $\operatorname{div}_\Sigma(\overline{(u_1, u_2)}) = 0$ and $\operatorname{div}((u_1, u_2, u_3)) = 0$ for the hydapp Stokes problem and the Stokes problem respectively; these constraints are subject to different Lipschitz constants and therefore give rise to different conditions for the iteration parameter α. Notice that for this problem the surface pressure in Σ is used as a Lagrangian multiplier, while for the Stokes problem the pressure in Ω should be used. The inclusion of the Coriolis term does not affect the convergence of the procedure.

Writing (13) in an explicit way yields

$$\begin{aligned} &u^{m+1} \in \mathbb{H}_0^1(\Omega), \\ &Xu^{m+1} - \mu\Delta u^{m+1} = -\operatorname{grad}_\Sigma(P^m) + f \in \mathbb{H}^{-1}(\Omega), \\ &p^{m+1} = p^m - \alpha \operatorname{div}_\Sigma(\overline{u^{m+1}}) \in L^2(\Sigma), \end{aligned} \tag{15}$$

where $p^m \in L^2(\Omega)$ is related to $p^m \in \mathrm{L}^2(\Sigma)$ by (12).

4. THE DISCRETE HYDAPP STOKES PROBLEM

4.1 A finite element method

An iteration procedure is presented that may be used to solve a discrete form of the hydapp Stokes problem. To fix ideas, in this subsection a discretization of Ω and Σ will be based on a finite element method. Let the volume Ω be divided into tetrahedra and let the surface Σ be covered with triangles. It is remarked that the subdivisions of Ω and Σ are in principle independent of each other, although it may be practical that the triangles that are used to cover Σ coincide with the upper sides of the tetrahedra on the surface of the domain Ω. For the basis functions $\phi_i \in H_0^1(\Omega)$ (i varies from $i=1$ to the number of nodes in the interior of Ω) we have: ϕ_i is linear in each tetrahedron; $\phi_i = 1$ at the interior node i and $\phi_i = 0$ at any other node. An internal approximation of $L^2(\Sigma)$ is provided by the basis functions $\eta_j \in L^2(\Sigma)$ (j varies from $j=1$ to the number of triangles in Σ), where η_j is the characteristic function of the jth triangle. Figure 2 shows an analogous subdivision for a 2D domain with a 1D surface. Thus we seek an approximation of the solution $\{u, p\}$ of (7), with p defined as in (11), of the form

$$u_h = \sum_i u_i \phi_i, \qquad p_h = \sum_j p_j \eta_j, \tag{16}$$

with $u_i = (u_{1i}, u_{2i})^T \in \mathbb{R}^2$ and $p_j \in \mathbb{R}$. For the unknown vectors we shall use the notation $v_h = (u_{11}, u_{12}, \ldots, u_{1I}, u_{2I}) \in \mathbb{R}^{2I}$ and $\pi_h = (p_1, \ldots, p_J) \in \mathbb{R}^J$.

We shall define the discrete form of algorithm (13) on account of the above discretization. Given the basis functions, the discrete forms of the Coriolis term and the Laplacian are obtained in the usual way by deriving the matrices X_h and $-\mu\Delta_h \in \mathbb{R}^{2I} \times \mathbb{R}^{2I}$ from the corresponding bilineaer forms in (13). Notice that X_h is a skew-symmetric matrix and that $-\mu\Delta_h$ is a symmetric positive definite (SPD) matrix. The discrete forms of the divergence operator and gradient operator are derived in a similar way and are denoted by $D_h \in \mathbb{R}^J \times \mathbb{R}^{2I}$ and its adjoint $D_h^* \in \mathbb{R}^{2I} \times \mathbb{R}^J$ respectively. These matrices can easily be defined in terms of the coefficients

$$\lambda_{ij}^k = \int_\Sigma \left(\frac{\partial}{\partial x_k} \int_0^h \phi_i \mathrm{d}z \right) \eta_j \mathrm{d}\Sigma \quad (k = 1, 2).$$

Then the Uzawa algorithm (13)/(15) for the discrete hydapp Stokes problem (7) takes the form

$$\begin{aligned} (X_h - \mu\Delta_h) v_h^{m+1} &= D_h^* \pi_h^m + f_h \in \mathbb{R}^{2I}, \\ \pi_h^{m+1} &= \pi_h^m - \alpha D_h v_h^{m+1} \in \mathbb{R}^J. \end{aligned} \tag{17}$$

The procedure is started with an arbitrary $\pi_h{}^0 \in \mathbb{R}^J$ and convergence of the procedure may be proven in the same manner as for problem (13) if α satisfies (14), provided the finite element structure is compatible, i.e. that $\ker D_h^* = 0$. Once the horizontal velocity u_h has been found from (17) and (16), the vertical velocity component can be derived from a discrete form of (9).

The evaluation of the surface pressure components π_j^{m+1} ($j = 1, \ldots, J$) at each m-iteration in (17) is explicit, because the characterisic functions η_j of the surface elements are orthogonal. To carry out a single m-iteration, it is necessary to solve an auxiliary coupled linear system whose matrix is $X_h - \mu\Delta_h$, which consists of a skew-symmetric and an SPD part. The iteration scheme that is described in Proposition 3 may be used to solve this system.

Proposition 3

Consider the problem of finding $v \in \mathbb{R}^k$ such that

$$(\Upsilon + \Lambda) v = f \in \mathbb{R}^k, \tag{18}$$

with Υ, $\Lambda \in \mathbb{R}^k \times \mathbb{R}^k$. Υ is a skew-symmetric matrix with $\| \Upsilon \|_2 \leq 1$ and Λ is a symmetric positive definite matrix. In order to solve the equation, the following iteration procedure is used. Starting with an arbitrary $v^{(0)} \in \mathbb{R}^k$, we define

$$\begin{aligned} v^{(1)} &= [(I + 2\beta\Lambda)^{-1}(-2\beta\Upsilon v^{(0)} + v^{(0)} + 2\beta f) + v^{(0)}]/2, \\ v^{(n+1)} &= (I + 2\beta\Lambda)^{-1}(-2\beta\Upsilon v^{(n)} + v^{(n-1)} + 2\beta f) \quad (n \geq 1), \end{aligned} \tag{19}$$

where $\beta \in \mathbb{R}$ is the iteration parameter. If $0 < \beta \leq 1$, then $v^{(n)}$ converges to v in $\mathbb{R}^k$ as $n \to \infty$ with an asymptotic rate of convergence

$$R \geq -\ln(\delta) \quad \text{with} \quad \delta = \frac{1}{\sqrt{1 + 2\beta\lambda_{\min}}},$$

where $\lambda_{\min}$ is the minimum eigenvalue of Λ.

Proof. See Appendix.

Scheme (19) is leap-frog with respect to the skew-symmetric term. The choice of the first iteration is the appropriate one for this multi-level method and avoids the tendency of the leap-frog method to 'decouple' solutions at alternate iterations. Therefore this modification improves the convergence. During the procedure an auxiliary system has to be solved as well whose matrix is the SPD matrix $I+2\beta\Lambda$. It is noticed that if the matrix Λ is the SPD part of the first equation of (17), then Λ may be decomposed into two matrix blocks of order I, each of which relates to one of the horizontal velocity components. The resulting SPD band matrix systems can often be dealt with by a direct method. If the two subsystems are still too large for a direct method, a variety of fast iteration procedures exist to solve SPD problems, such as the conjugate gradient method, the successive overrelaxation method or Chebyshev polynomial acceleration procedures.[14,15]

The discretization of both Ω and Σ should result in approximations u_h and p_h, that have a comparable order of precision with respect to the solutions u and p of problem (7). Therefore it is sufficient to let the sides of triangles that divide the surface Σ have side lengths comparable with those of the tetrahedra that divide the volume Ω. In this respect it is noticed that in general a finite element solution for the Stokes problem is found by using an external approximation for the velocity components in order to compensate for the large number of degrees of freedom of the discrete pressure, which for the Stokes problem equals the number of elements in Ω. For the hydapp Stokes equations this is often not necessary, because here the number of degrees of freedom of the discrete pressure is much less, being the number of triangles in Σ, so that the compatibility condition can be satisfied more easily.

4.2. A finite difference method

The use of an unstructured finite element grid may be costly in terms of CPU time for three-dimensional general circulation problems which demand a high grid resolution. Therefore we shall discuss a finite difference method that is based on the Arakawa C-grid.[16] This grid is often used in geophysical fluid dynamics.[2,4,6] In the C-grid the basis functions for the velocity components and pressure are the characteristic functions of parallelepipeds in the domain Ω, the so-called u-, v-, w- and P-cells (i, j, k). They are staggered with respect to each other (Figure 3). Thus each of these basis functions is an element of $L^2(\Omega)$. In our case we shall also distinguish rectangles, the so-called p-cells (i, j) on Σ, which coincide with the upper sides of the P-cells on the surface of Ω. The basis functions

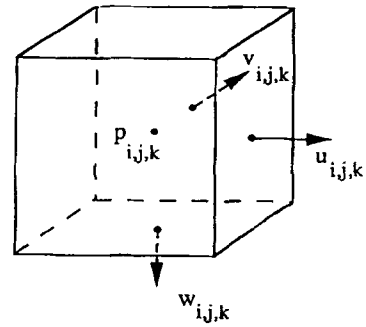

Figure 3. Arakawa C-grid P-cell in 3D; u_{ijk}, v_{ijk}, and w_{ijk} are drawn at the centers of the staggered U-, V- and W-cells respectively

in Σ are the characteristic functions on the p-cells, which are elements of $L^2(\Sigma)$. The domain Ω is assumed to be filled with P-cells. Thus we seek approximate solutions of the form

$$\begin{aligned} u_h &= \sum_{ijk} u_{ijk} U_{ijk}, & v_h &= \sum_{ijk} v_{ijk} V_{ijk}, & w_h &= \sum_{ijk} w_{ijk} W_{ijk}, \\ p_h &= \sum_{ij} p_{ij} q_{ij}, & P_h &= \sum_{ijk} P_{ijk} Q_{ijk}, \end{aligned} \tag{20}$$

where U_{ijk}, V_{ijk}, W_{ijk}, Q_{ijk} and q_{ij} denote the characteristic functions with respect to the corresponding cells. The finite difference operator in the i-direction ($i = 1, 2, 3$) is defined as

$$(\delta_i \phi)(x) = \frac{\phi(x + \frac{1}{2}\Delta x_i) - \phi(x - \frac{1}{2}\Delta x_i)}{\Delta x_i}. \tag{21}$$

We shall define the discrete form of the Uzawa algorithm given by (13) on account of the above discretization. Given the basis functions, the discrete forms of the Coriolis term and Laplacian are obtained by deriving the matrices X_h and $-\mu\Delta_h \in \mathbb{R}^{2I} \times \mathbb{R}^{2I}$ from the corresponding bilinear forms in (13) and using the finite difference operator (21). The Coriolis factor χ is, like the pressure, approximated in terms of the P-cell basis functions. In particular, for the Coriolis term we get

$$\begin{aligned} &\frac{1}{\Delta x \Delta y \Delta z} \int_\Omega \left(\sum_{pqr} -\chi_{pq} Q_{pqr} \right) \left(\sum_{pqr} v_{pqr} V_{pqr} \right) U_{ijk} \, d\Omega \\ &\qquad = \tfrac{1}{4}[-\chi_{ij}(v_{ijk} + v_{i,j-1,k}) - \chi_{i+1,j}(v_{i+1,j,k} + v_{i+1,j-1,k})], \\ &\frac{1}{\Delta x \Delta y \Delta z} \int_\Omega \left(\sum_{pqr} \chi_{pq} Q_{pqr} \right) \left(\sum_{pqr} u_{pqr} U_{pqr} \right) V_{ijk} \, d\Omega \\ &\qquad = \tfrac{1}{4}[\chi_{ij}(u_{ijk} + u_{i-1,j,k}) + \chi_{i,j+1}(u_{i,j+1,k} + u_{i-1,j+1,k})] \end{aligned} \tag{22}$$

and one may notice that the resulting matrix X_h is skew-symmetric. If we apply the discrete Uzawa algorithm for convenience to the two-dimensional case, i.e. with one horizontal and one vertical

dimension, then we obtain the system of equations

$$-\mu\left(\frac{u_{i+1,k}^{m+1}-2u_{ik}^{m+1}+u_{i-1,k}^{m+1}}{\Delta x^2}+\frac{u_{i,k+1}^{m+1}-2u_{ik}^{m+1}+u_{i,k-1}^{m+1}}{\Delta z^2}\right)=-\frac{p_{i+1}^m-p_i^m}{\Delta x}+f_{ik},$$
$$p_i^{m+1}=p_i^m-\alpha\frac{\sum_{k=1}^{K(i)}u_{ik}^{m+1}\Delta z-\sum_{k=1}^{K(i-1)}u_{i-1,k}^{m+1}\Delta z}{\Delta x}, \tag{23}$$

where $K(i)$ is the number of u-cells which are below and between the ith and the $(i+1)$th p-surface. The convergence of the procedure may be proven in the same manner as for problem (13) if α satisfies (14). Once the horizontal velocity u_h has been found, the vertical velocity component is derived form (9). Here its evaluation is explicit and is expressed as

$$w_{ik}=\sum_{\kappa=1}^{k}u_{i\kappa}-\frac{u_{i-1,\kappa}}{\Delta x}\Delta z \quad (i=1,\ldots,I;\ k=1,K(i)). \tag{24}$$

The extension of (23) and (24) to the three-dimensional case and the inclusion of the Coriolis term (22) in (23) are straightforward. Then, as for scheme (17), to carry out a single m-iteration, it is necessary to solve an auxiliary coupled linear system whose matrix consists of a skew-symmetric and an SPD part. This system can be solved with algorithm (19).

5. THE HYDAPP EVOLUTION NAVIER–STOKES PROBLEM

A similar analysis for the hydapp evolution Navier–Stokes problem, i.e. for problem (6) with $r>0$, is more complicated than what has been presented in Section 3 for the hydapp Stokes problem. Such an analysis is outside the scope of this paper, where we wish to arrive at applicable iteration schemes to solve a discrete form of this problem. Therefore derivations will be presented only for the linearized version of these equations and the results will be extended to the non-linear case.

We introduce the space

$$\mathbb{Y}=\{(c_1,\ c_2,\ c_3)\in H_0^1(\Omega)\times H_0^1(\Omega)\times Z\},$$

where the space Z is defined as in (9), and we define a continuous trilinear form b on $\mathbb{Y}\times\mathbb{H}_0^1(\Omega)\times\mathbb{H}_0^1(\Omega)$ by

$$b(c,\ u,\ v)=\frac{1}{2}\sum_{j=1}^{2}\int_\Omega\left(c_1\frac{\partial u_j}{\partial x_1}v_j+c_2\frac{\partial u_j}{\partial x_2}v_j+c_3\frac{\partial u_j}{\partial x_3}v_j\right.$$
$$\left.-c_1u_j\frac{\partial v_j}{\partial x_1}-c_2u_j\frac{\partial v_j}{\partial x_2}-c_3u_j\frac{\partial v_j}{\partial x_3}\right)\mathrm{d}\Omega, \tag{25}$$

which is skew-symmetric in its last two arguments. Further, let T be a positive real number, H be a Hilbert space and $L^2(0,\ T;\ H)$ denote the space of L^2-integrable functions from $[0,\ T]$ into H, which is a Hilbert space with norm

$$\left(\int_0^T\mathrm{d}t\|f(t)\|_H^2\right)^{1/2}.$$

The following weak formulation is considered:

$$\begin{cases} \text{given } f \in \mathbb{L}^2(0,\ T;\ \mathbb{L}^2(\Omega)),\ c \in \mathbb{Y} \text{ and } u_0 \in V, \\ \text{find } u \in \mathbb{L}^2(0,\ t;\ V) \quad \text{such that} \\ r\left(\frac{\mathrm{d}}{\mathrm{d}t}(u,\ v)_{\mathbb{L}^2(\Omega)} + b(c,\ u,\ v)\right) + a(u,\ v) = L(v), \quad \forall v \in V, \\ u(0) = u_0, \end{cases} \tag{26}$$

where $a(.,.)$ and $L(.)$ are defined as in (7). Although u belongs to $\mathbb{L}^2(0, T; V)$ the initial condition makes sense; its meaning is explained in Reference 13 (pp. 253–254). The existence and uniqueness of a solution of (26) may be proven on account of the results derived in Section 3 and by proceeding in a similar fashion as for the evolution Stokes problem Reference 13, pp. 247–269.

Problem (26) suggests a weak formulation for the hydapp evolution Navier–Stokes problem which is based on replacing the constant advection velocity $c \in \mathbb{Y}$ in $b(c, u, v)$ by $(u, u_3) = (u_1, u_2, u_3) \in \mathbb{Y}$, where $u_3 \in Z$ is given by (9). It is not difficult to see that on account of the kinematic condition (see (4))

$$b((u, u_3), u, v) = \sum_{j=1}^{2} \int_\Omega u_1 \frac{\partial u_j}{\partial x_1} v_j + u_2 \frac{\partial u_j}{\partial x_2} v_j + u_3 \frac{\partial u_j}{\partial x_3} v_j, \quad \forall v \in V.$$

The substitution of c by (u, u_3) will be carried out when a discrete form of (26) is considered and we will not seek any further the exact conditions under which this substitution is justified.

We shall consider a discrete form of (26). The time dependence of the variables will be indicated by a superscript n and the length of the time step by a constant $\tau > 0$. There exist many time discretization schemes that can be applied. Here we shall consider a procedure which is suggested by scheme (19). Let there be given an internal or external stable and convergent approximation of the space V, say V_h, with appropriate prolongation and restriction operators. V_h is assumed to be finite-dimensional. Together with V_h, one can define an approximation W_h of $\mathbb{H}_0^1(\Omega)$. Essentially, the elements u_h of W_h are of exactly the same type as the elements u_h of V_h, but no divergence condition is imposed. Then, by using scheme (19), the time integration is started with any $u_h^0 \in V_h$ and u_h^n $(n \geq 1)$ is the solution in V_h of

$$\begin{aligned} &r\left(\frac{1}{\tau}(u_h^1 - u_h^0,\ v_h)_{\mathbb{L}^2(\Omega)} + b_h((u_h^0,\ w_h^0),\ u_h^0,\ v_h)\right) \\ &\qquad + (X_h u^0,\ v_h)_{\mathbb{L}^2(\Omega)} + \mu(2u_h^1 - u_h^0,\ v_h)_{W_h} = (f_h,\ v_h)_{\mathbb{L}^2(\Omega)}, \quad \forall v_h \in V_h, \\ &r\left(\frac{1}{2\tau}(u_h^{n+1} - u_h^{n-1},\ v_h)_{\mathbb{L}^2(\Omega)} + b_h((u_h^n,\ w_h^n),\ u_h^n,\ v_h)\right) \\ &\qquad + (X_h u_h^n,\ v_h)_{\mathbb{L}^2(\Omega)} + \mu(u_h^{n+1},\ v_h)_{W_h} = (f_h,\ v_h)_{\mathbb{L}^2(\Omega)}, \quad \forall v_h \in V_h \quad (n \geq 1). \end{aligned} \tag{27}$$

The computation of the elements u_h^m of V_h is not easy. The difficulty is connected with the constraint '$\mathrm{div}_\Sigma(\bar{u}) = 0$' built into the definition of the space V_h; actually, the situation is the same as in Section 3 for the hydapp Stokes problem. Therefore the problem is reformulated in the space W_h. Let X_h be the space of step functions on Σ. In a similar fashion as in Section 3, one may show that if u_h^m is solution of (27), there exists a step function $p_h^m \in X_h$ such that

$$\begin{aligned} &r\left(\frac{1}{2\tau}(u_h^{n+1} - u_h^{n-1},\ v_h)_{\mathbb{L}^2(\Omega)} + b_h((u_h^n,\ w_h^n),\ u_h^n,\ v_h)\right) \\ &\qquad + (X_h u_h^n,\ v_h)_{\mathbb{L}^2(\Omega)} + \mu(u_h^{n+1},\ v_h)_{W_h} + (p_h^n,\ \mathrm{div}_{\Sigma_h}(\overline{v_h}))_{L^2(\Sigma)} \\ &\qquad = (f_h,\ v_h)_{\mathbb{L}^2(\Omega)}, \quad \forall v_h \in W_h, \end{aligned} \tag{28}$$

with a similar result for the first iteration of (27).

The resolution of (28) can be done by applying the Uzawa algorithm. Assuming that the elements of time steps n and $n-1$ have been computed, we must then compute the unknowns $u_h^{n+1} \in V_h$; and $p_h^{n+1} \in X_h$. They will be obtained as the limits of two sequences of elements

$$u^{n+1,m} \in W_h \quad \text{and} \quad p^{n+1,m} \in X_h, \quad m = 0, 1, \ldots, \infty.$$

When $p_h^{n+1,m}$ is known, using the same notation as in (16) and (17), $u_h^{n+1,m+1}$ and $p_h^{n+1,m+1}$ ($m \geq 0$) are defined by

$$\begin{aligned} (S_h - \mu\Delta_h)v_h^{n+1,m+1} &= D_h^* \pi_h^{n+1,m} + g_h^n \in \mathbb{R}^{2I}, \\ \pi_h^{n+1,m+1} - \pi_h^{n+1,m} - \alpha D_h v_h^{n+1,m+1} &\in \mathbb{R}^J, \end{aligned} \tag{29}$$

where the explicit terms in (28) have been collected in g_h^n and where the SPD matrix S_h is associated with the bilinear form $(u_h^{n+1}, v_h)_{\mathbb{L}^2(\Omega)}$ in (28). In the particular case of the finite difference formulation based on the C-grid, S_h is the identity matrix. The procedure is started with an arbitrary $\pi_h^{n+1,0} \in \mathbb{R}^J$, e.g. $\pi_h^{n+1,0} = \pi^n$. When u_h^{n+1} has been computed, the vertical velocity w_h^{n+1} is found from a discrete form of (9). Further, as for the hydapp Stokes problem, to carry out a single m-iteration, it is necessary to solve an auxiliary coupled linear system. However, in this case the system is SPD and does not contain a skew-symmetric part.

The discrete trilinear form b_h of b defined by (25) is skew-symmetric in its last two arguments. If we assume for a moment that its first argument in (28) is a constant $c_h \in \mathbb{V}_h$, then from Proposition 3 it follows that $u_h^n \in V_h$ will converge to the stationary solution $u_h^\infty \in V_h$ when the time step $\tau > 0$ is taken sufficiently small. Therefore, in practice, Proposition 3 provides a necessary stability criterion where the upper bound for the time step is given by the norm of the skew-symmetric matrix which results from the non-linear and the Coriolis term in (28).

6. SOME REMARKS

We have discussed the application of the Uzawa method to solve the variational formulations (7) and (26), but there exist several other methods that can be used. A method that is closely related to the Uzawa method is the Arrow–Hurwicz algorithm.[12] One may also use a penalty technique or the augmented Lagrangian technique.[17–19] The Uzawa method may be considered to be the simplest of these methods. An advantage of the Arrow–Hurwicz algorithm over the Uzawa method is that during the iteration procedure to boundary value problem is solved, but the viscosity term is treated explicitly at each iteration. With the augmented Lagrangian technique, basic methods such as Uzawa and Arrow–Hurwicz can be accelerated considerably. It is remarked that the use of non-constant turbulent viscosity coefficients or the inclusion of islands in Ω does not affect the overall procedure of these algorithms.

Compared with the way the hydapp Stokes problem was solved with (18) and (19), to solve the evolution hydapp Navier–Stokes problem, the order of the algorithms has been interchanged by putting (19) on top of (29). Of course, the latter procedure can also be used to solve the hydapp Stokes problem, by interpreting the time step as an iteration parameter and neglecting the non-linear term in (28). In fact, in general this procedure is to be preferred, because the Uzawa algorithm (29) is applied to a problem without a skew-symmetric part and this gives the possibility to accelerate the convergence more strongly.

An iteration procedure has been presented to solve the discrete hydapp Navier–Stokes problem with homogeneous Dirichlet boundary conditions. There are two other configurations of boundary conditions that are of particular importance in geophysical fluid problems. The first one is a Neumann condition at the surface Σ that specifies $\partial u_1/\partial z$ and $\partial u_1/\partial z$, with which wind stress can be expressed. In

this case, instead of V in the variational formulation (7), the space $\{v \in \mathbb{H}^1(\Omega) \mid \operatorname{div}_\Sigma(\bar{v}) = 0, \gamma v \mid_\Gamma = 0\}$ is used. It may be verified that with this Neumann condition the Lipschitz constant for the discrete divergence operator in (8) is the same as for the homogeneous Dirichlet problem, so that the convergence criterion (14) for the Uzawa algorithm is unaffected. The second type of boundary condition that is of interest is a non-homogeneous Dirichlet condition at the boundary part Γ_L specifying lateral inflow and outflow. The specification must be such that the net flux through Γ_L is zero. One may prove, in a similar way as for the Stokes problem[13] and by using Proposition 1, that this condition is necessary and sufficient for the existence and uniqueness of a solution. Further, the adapatation of one of the algorithms mentioned before for such a non-homogeneous problem is straightforward.[18]

The time integration scheme (27) was chosen to discretize (26), but other schemes can be applied, such as a Crank–Nicolson scheme, from which a similar problem to (28) would result. When the Coriolis term is to be treated (semi-) implicitly, at every time step a hydapp Stokes problem with Coriolis term must be solved as described in Section 4. In the last paragraph of the previous section a necessary condition on the length of the time step was given. In most applications, however, the hydapp Navier–Stokes equations must be coupled to a heat and/or salinity equation. Although the rigid lid boundary condition eliminates the highest-frequency surface wave components, it is mentioned that in the baroclinic case the high-frequency internal gravity waves will often put the severest condition on the length of the time step. If this is the case, it may be necessary to consider more cost-effective time integration schemes for the treatment of these waves. We refer to References 20 and 21 and references cited therein for a discussion on this subject.

7. NUMERICAL EXAMPLES

7.1. A two-dimensional hydapp Stokes example

The hydapp Stokes problem will be solved with finite elements and with finite differences based on the C-grid. We will consider a two-dimensional domain Ω with its one-dimensional surface Σ. Thus there is only one horizontal velocity component u and there is no Coriolis effect. For the viscosity coefficient or Ekman number we take $\mu = 1$. The boundary condition at the surface Σ is taken to be Neumann, say $\partial u/\partial z = 10$, expressing wind stress, and at the bottom Γ_b and the lateral boundary Γ_L to be Dirichlet with $u = 0$, expressing no slip.

To solve the problem with finite elements, the domain Ω is covered with triangles and its surface Σ is divided into intervals (see Figure 2). The internal approximation of the space $\{v \in H^1(\Omega) \mid v \mid_\Gamma = 0\}$ is based on the same type of basis functions as described in Section 4.1. The discretization consists of a triangulation of Ω into 6141 elements; the number of variable nodes is 3045. The surface Σ is subdivided into 100 equidistant p-intervals. As mentioned before, with a Neumann condition at the surface the Lipschitz constant for the discrete divergence operator in (8) is the same as for the homogeneous Dirichlet problem, so that the convergence criterion (14) for the Uzawa algorithm is unaffected.

The problem is solved with scheme (17) without the Coriolis term. At each m-iteration the first equation of (17) is solved with a direct method. The procedure is initialized with $p^0 = 0$ and the stop criterion is taken to be

$$\|\operatorname{div}_{\Sigma_h}(\overline{u_h^{m+1}})\|_{L^2(\Sigma)} \leq \varepsilon = 10^{-5}.$$

This criterion is satisfied after 43 Uzawa m-iterations when the iteration parameter is taken as $\alpha = 0{\cdot}93 \times 2\mu/\mathscr{C}^2$. The number of m-iterations is given as a reference value. As mentioned, various methods exist to accelerate the Uzawa algorithm and one can easily reduce this number. Figure 4

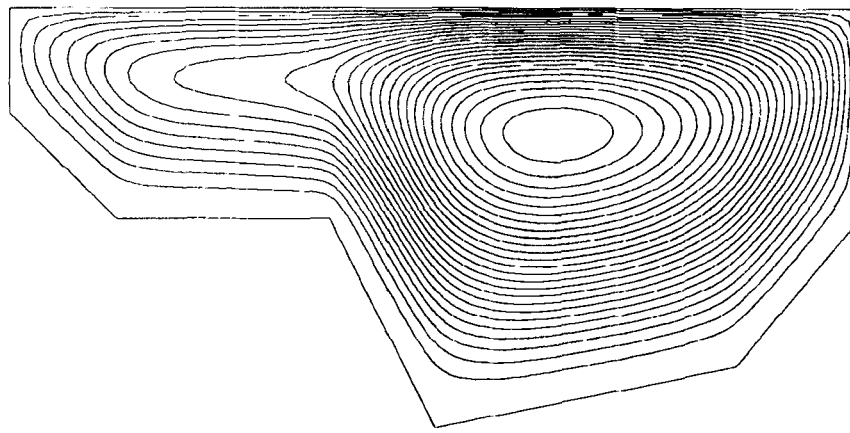

Figure 4. Streamlines resulting from a finite element calculation in a 2D domain. Notice the relatively strong vertical velocity at the vertical side of the domain, because no boundary condition for this velocity component is specified on this side

shows the resulting streamlines of the flow. Notice the relatively strong vertical velocity near the lateral parts of the boundary. This is explained by the fact that for the hydapp Stokes problem no Dirichlet condition at a vertical side can be specified for this velocity component, as remarked near the end of Section 2.

The same problem is solved with the finite difference method based on the C-grid as described in Section 4.2. The domain is covered with P-cells. The bottom cannot be exactly resolved with these cells, but it is staircase-like approximated. Further, when using the C-grid, Dirichlet and Neumann conditions for u_h cannot be specified exactly on horizontal parts of the boundary, but they are prescribed with precision $O(\Delta z^2)$ in the usual way. The maximum number of P-cells in a row is 100 and in a column 50. The number of internal u-cells in Ω is 3412, which is about the same as the number of variable nodes with which the finite element calculation was carried out. The number of equidistant p-intervals subdividing Σ is 100, as in the finite element calculation. The stop criterion is

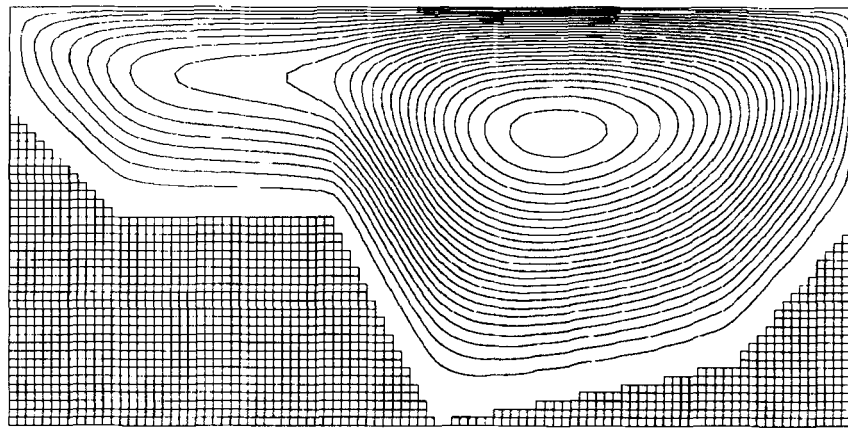

Figure 5. Streamlines resulting from a finite difference calculation in a 2D domain. P-cells are shown outside the domain. The bottom Γ_b is staircase-like. The result is hardly different from that of the finite element calculation shown in Figure 4.

satisfied after 59 m-iterations with scheme (23) with $\alpha = 0{\cdot}93 \times 2\mu/\mathscr{C}^2$. Figure 5 shows the streamlines of the flow. The result hardly differs from that of the finite element case.

The unstructured finite element method permits a better approximation of the boundary than the finite difference method and for boundary layer problems it is to be preferred. The first method, however, uses more computer operations than the second one. This is mainly due to the evaluation of the divergence and gradient operators in (17) at each interation. As mentioned, because of the anisotropic nature of the hydrostatic approximation problem, it is advantageous to use a discretization which is structured to the vertical direction in such a way that the integration in the vertical direction can be done easily. This is even more important in the non-linear case, where at each iteration the vertical velocity component has to be evaluated as well from a discrete form of (9). The Arakawa C-grid formalism resulting in discretizations (22)–(24) is very suitable for this purpose. Another possibility in the 3D case is the use of a finite element structure defined on the horizontal surface Σ which is compatible for the classical 2D Stokes problem and a finite difference extension in the vertical direction.

7.2. A simulation of the general circulation in Lake Neuchâtel

Lake Neuchâtel is a quasi-rectangular body of water in western Switzerland. Its longest axis is directed SW–NE. The maximum length is 38·3 km, the average width 5·7 km and the maximum depth 142 m. The bathymetry of the lake is like an 'elongated bathtub' with a bump centred in the NE region (Figure 6). This bump, called la Motte, is a rather steep mountain with its peak only 10 m below the water surface. The dominant wind is le Vent, a SW wind blowing along the long axis of the lake. More information about the morphology of the lake can be found in References 22 and 23.

A number of studies have been carried out in the past that relate to the general circulation of Lake Neuchâtel. Barotropic processes were addressed by Zuur and Dietrich[24] using the Sandia Ocean Modeling System model. A numerical simulation of transport and sedimentation of suspended particles was performed by Thunus *et al.*,[25] where the methods described in this paper were applied to simulate the currents. Here we will describe a short simulation to illustrate the performance of the derived iteration schemes.

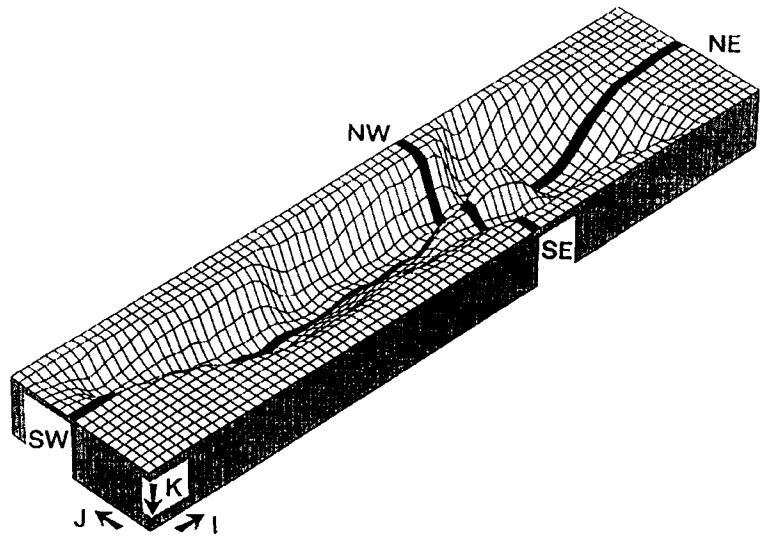

Figure 6. A 3D perspective of the lake topography. The location of the SW–NE vertical section in Figure 7(c) and 8(c) is shown.

To simulate the general circulation in the lake under autumnal conditions, the effect of thermal stratification must be included. Therefore the evolution hydapp Navier–Stokes equations must be coupled with an equation of state and a heat equation. By using the time integration described in the previous section, we get the following system of equations expressed in terms of the continuity equations in dimensional form:

$$\frac{u^{n+1}-u^{n-1}}{2\Delta t}+(\vec{v}^n\cdot\nabla)u^n-\chi v^n=-\frac{\partial P^{n+1}}{\partial x}+A_{\mathrm{H}}\left(\frac{\partial^2 u^{n+1}}{\partial x^2}+\frac{u^{n+1}}{y^2}\right)+A_{\mathrm{V}}\frac{\partial^2 u^{n+1}}{z^2},$$

$$\frac{v^{n+1}-v^{n-1}}{2\Delta t}+(\vec{v}^n\cdot\nabla)v^n-\chi u^n=-\frac{\partial P^{n+1}}{\partial x}+A_{\mathrm{H}}\left(\frac{\partial^2 v^{n+1}}{\partial x^2}+\frac{\partial^2 v^{n+1}}{\partial y^2}\right)+A_{\mathrm{V}}\frac{\partial^2 v^{n+1}}{z^2},$$

$$\frac{\partial P^{n+1}}{\partial z}=\rho^n g,\quad \text{with } \rho^n=\rho_0(1-\gamma T^n), \tag{30}$$

$$\frac{\partial u^{n+1}}{\partial x}+\frac{\partial v^{n+1}}{\partial y}+\frac{\partial w^{n+1}}{\partial z}=0,$$

$$\frac{T^{n+1}-T^{n-1}}{2\Delta t}+(\vec{v}^n\cdot\nabla)T^n=K_{\mathrm{H}}\left(\frac{\partial^2 T^{n+1}}{\partial x^2}+\frac{\partial^2 T^{n+1}}{\partial y^2}\right)+K_{\mathrm{V}}\frac{\partial^2 T^{n+1}}{\partial z^2},$$

with, according to (27), a similar expression for the first time step. Here the symbols have the following meaning:

x, y, z	spatial co-ordinates in a left-handed Cartesian system (z-axis points downwards) [L]
t	time [T]
T	temperature [Θ]
u, v, w	velocity components ($\vec{v}=(u, v, w)$) [L T^{-1}]
P	kinematic pressure [L^2 T^2]
ρ	normalized density (ρ_0 is reference density)
g	effective gravitational acceleration [L T^{-2}]
$A_{\mathrm{H}}, A_{\mathrm{V}}, K_{\mathrm{H}}, K_{\mathrm{V}}$	turbulent viscosity and diffusion coefficients [L^2 T^{-1}]
χ	constant Coriolis parameter [T^{-1}]
γ	coefficient of thermal expansion [Θ^{-1}].

For the spatial discretization the Arakawa C-grid is used as described in Section 4.2. The volume of the lake is embedded in a rectangular box which is filled with P-cells. A horizontal plane of this box contains 70 × 18 P-cells (Figure 6), the area of each P-cell being 526 × 526 m^2. In the vertical direction there are 20 layers of P-cells, the thickness of each layer being 7·1 m. The temperature is, like the pressure, discretized in terms of the P-cell basis functions. At each time step, first the pressure P is decomposed as in (5) into a non-hydrostatic surface pressure part and a hydrostatic part resulting from the non-uniform density field. Then the first four equations of (30) are solved with scheme (28)/(29), with the slight difference that the horizontal viscosity terms are treated explicitly in this scheme, i.e. a combination of the Uzawa and Arrow–Hurwicz algorithms is used. This has the advantage that during every Uzawa/Arrow–Hurwicz iteration at each horizontal position a small boundary value problem of the order of the number of horizontal layers has to be solved that relates to the vertical viscosity component, instead of one large boundary value problem that relates to the whole viscosity term. After the velocity field has been updated, the heat equation is evaluated to obtain the new temperature field.

In order to identify some typical hydrodynamic features in the lake, the following simulation is performed. At the start of the run the lake is at rest and is thermally stratified: the temperature decreases linearly from 10°C at the surface down to 5°C at maximum depth. Then a spatially uniform SW wind blowing along the main axis is turned on with a constant wind speed. This wind lasts for 12 h. After 12 h the wind is turned off and the run is contained for another 12 h.

The wind-induced stress at the surface of the lake is related to the wind speed by a bulk aerodynamic formula, which results in a Neumann boundary condition for the horizontal components of the velocity at the surface:

$$\rho_0 A_V \left(\frac{\partial u}{\partial z}, \frac{\partial v}{\partial z}\right)^T = \rho_a C_d \sqrt{(U_{10}^2 + V_{10}^2)}(U_{10}, V_{10},)^T \quad \text{on } \Sigma,$$

where ρ_a is the air density, $(U_{10}, V_{10})^T$ is the air velocity at an elevation of 10 m above the lake surface and C_d is a drag coefficient. At the bottom Γ_b and the lateral boundary Γ_L the boundary conditions for the horizontal velocity components are taken to be Dirichlet with $u = v = 0$. The parameters used in the calculation have the following values:

$\rho_0 = 1000$ kg m^{-3},	$A_H = 10$ m^2 s^{-1},	$\rho_a = 1{\cdot}225$ kg m^{-3},
$\chi = 1{\cdot}05 \times 10^{-4}$ s^{-1},	$A_V = 2{\cdot}5 \times 10^{-3}$ m^2 s^{-1}	$C_d = 0{\cdot}004$,
$g = 9{\cdot}8$ m s^{-2},	$K_H = 10$ m^2 s^{-1},	$\gamma = 0{\cdot}2 \times 10^{-3}$,
$\Delta t = 120$ s,	$K_V = 2{\cdot}5 \times 10^{-3}$ m^2 s^{-1}.	

The wind speed is $(U_{10}, V_{10}) = (7{\cdot}5, 0)$ m s^{-1} for $0 \leq t \leq 12$ h and $(U_{10}, V_{10}) = 0$ for $12 < t \leq 24$ h. The values for the viscosity and drag coefficients were taken from Reference 26.

For this simulation the time step is not so much limited by the explicit treatment of the Coriolis term but by the internal gravity waves. The total number of time steps to arrive at an integration of 24 h is 540. As the initial pressure for iteration procedure (29), the pressure which resulted from the previous time step is taken. This means in particular that if the flow field were stationary at a given time, only one m-iteration would be performed. The mean number of m-iterations over the 540 steps is 7·86 per time step. The whole calculation takes less than 4 min on a VAX AXP system.

Results are presented at two points in time, after 12 h in Plate 1 and after 24 h in Plate 2. For brevity, only two among the 20 depth levels and one of the 18 vertical slices in the length direction of the lake are displayed. The size of the arrows at a given level/slice is scaled to the maximum velocity that occurs at that level/slice and its magnitude is denoted under the corresponding plot. K and J denote the number of the depth level and of the cross-section respectively. K increases from surface to bottom from $K = 1$ to 20 and J increases from SE to NW from $J = 1$ to 70.

After 12 h of wind forcing, near the surface and away from the boundary the velocity field is deflected to the right relative to the SW wind owing to the Coriolis acceleration (Plate 1(a)). The angle of this deflection agrees with the theoretical value of 45°, which is the limiting value in the Ekman layer when the surface is approached.[7] As the net horizontal flow in the upper layers is directed eastward, upwelling is induced in the west part and downwelling in the east part of the lake. This can clearly be seen from the horizontal temperature distribution in Plate 1(a). Thus a vortex in the vertical west–east plane has been set up by the wind, which is depicted in the vertical cross-section in Plate 1(c). After 12 h the wind is turned off and in Plate 2 the situation is shown 12 h later. During the 12 h without wind forcing, the currents in the middle of lake have horizontally propagated clockwise with inertial period $2\pi/\chi = 16{\cdot}6$ h owing to the Coriolis acceleration. A vortex appears in the NE part of the lake as a result of the existence of the topographic feature 'la Motte'. In the vertical direction the lake is subdivided into two oppositely rotating cells, epilimnetic and hypolimnetic, owing to the thermal stratification (Plate 2(c)).

8. CONCLUDING REMARKS

The numerical treatment of the hydrostatic approximation Navier–Stokes equations based on a reformulation of the original continuity equations has a number of advantages. In contrast with other formulations, the boundary value problem that must be solved at each time step relates to the horizontal velocity components only, for which the boundary conditions are specified and do not have to be approximated. This leads to more accurate results. The reformulation permits a variational formulation, the discrete form of which can be solved with various well-known techniques that have been developed in the past to solve the full Navier–Stokes problem. Although the derivation of the numerical method is based on the implicit treatment of the pressure, Coriolis and viscosity terms, to find the solution, explicit iterative methods are used. In this fashion, fast algorithms can be defined, in particular when the spatial discretization is appropriately structured in the vertical direction.

ACKNOWLEDGEMENTS

The author warmly thanks H. -H. Naegeli for thoroughly reviewing the manuscript and C. Cuvelier and V. Thunus for their helpful comments. This research was initiated with the support of the Swiss National Science Foundation (grant 2.055.086) and continued within the framework of the PROSPER programme (University of Neuchâtel, Switzerland) with the support of the Swiss Environmental Protection Office.

APPENDIX: PROOF OF PROPOSITION 3

First we will consider an iterative scheme which is slightly different from (19). Starting with $\varphi^{(0)} = v^{(0)}$, we define

$$\begin{aligned} \varphi^{(1)} &= \varphi^{(0)}, \\ \varphi^{(n+1)} &= (I + 2\beta\Lambda)^{-1}(-2\beta\Upsilon\varphi^{(n)} + \varphi^{(n-1)} + 2\beta f) \quad (n \geq 1). \end{aligned} \tag{31}$$

Let $\varepsilon^{(n)} = \varphi^{(n)} - v$ $(n \geq 0)$. By introducing the vector $\omega^{(n)} = \varepsilon^{(n-1)}$ $(n \geq 1)$, from (18) and (31) we derive

$$\begin{pmatrix} \varepsilon^{(n+1)} \\ \omega^{(n+1)} \end{pmatrix} = \begin{pmatrix} (I + 2\beta\Lambda)^{-1} & 0 \\ 0 & I \end{pmatrix} \begin{pmatrix} -2\beta\Upsilon & I \\ I & 0 \end{pmatrix} \begin{pmatrix} \varepsilon^{(n)} \\ \omega^{(n)} \end{pmatrix} \quad (n \geq 1). \tag{32}$$

It is readily verified that the iteration matrix is non-singular. Let $\xi = (\xi_1, \xi_2)^{\mathrm{T}} \in C^{2k}$ be any eigenvector of this matrix and let ϑ be a corresponding eigenvalue, i.e.

$$\begin{pmatrix} -2\beta\Upsilon & I \\ I & 0 \end{pmatrix} \begin{pmatrix} \xi_1 \\ \xi_2 \end{pmatrix} = \vartheta \begin{pmatrix} I + 2\beta\Lambda & 0 \\ 0 & I \end{pmatrix} \begin{pmatrix} \xi_1 \\ \xi_2 \end{pmatrix} \quad \text{or} \quad \begin{cases} -2\beta\Upsilon\xi_1 + \vartheta^{-1}\xi_1 = \vartheta(I + 2\beta\Lambda)\xi_1. \\ \xi_1 = \vartheta\xi_2 \end{cases}$$

By taking the dot product in C^k of the first equation with ξ_1 we get

$$-2\beta(\Upsilon\xi_1, \xi_1) + \vartheta^{-1}\|\xi_1\|_2^2 = \vartheta(\|\xi_1\|_2^2 + 2\beta(\Lambda\xi_1, \xi_1)).$$

Υ is a skew-symmetric matrix with $\|\Upsilon\| \leq 1$. Therefore, $(\Upsilon\xi_1, \xi_1)$ is pure imaginary and $|(\Upsilon\xi_1, \xi_1)| \leq \|\xi_1\|_2^2$. This means, there exists $\eta \in \mathbb{R}$ with $|\eta| \leq 1$ such that $(\Upsilon\xi_1, \xi_1) = i\eta\|\xi_1\|_2^2$. Λ is a symmetric positive definite matrix with minimum eigenvalue $\lambda_{\min} > 0$. So, there exists

$\alpha \in \mathbb{R}$ with $\alpha \geq \lambda_{\min}$ such that $(\Lambda\xi_1, \xi_1) = \alpha\|\xi_1\|_2^2$. By combining these equations it follows that ϑ is a solution of

$$(1 + 2\beta\alpha)\vartheta^2 + 2i\beta\eta\vartheta - 1 = 0,$$

from which we find that if $0 < \beta \leq 1$, then $|\vartheta| \leq \delta < 1$.

As the spectral radius of the iteration matrix $\rho \leq \delta < 1$, the iteration matrix is convergent. Then, it is well known that for every $\varepsilon > 0$ ($\varepsilon << 1$) there exists $\kappa \geq 1$ such that

$$\|\varepsilon^{(n+1)}\|_2^2 + \|\omega^{(n+1)}\|_2^2 \leq \kappa^2(\rho + \varepsilon)^{2n}(\|\varepsilon^{(1)}\|_2^2 + \|\omega^{(1)}\|_2^2) \quad (n \geq 0).$$

Now, one may verify that $v^{(n)} = (\varphi^{(n+1)} + \varphi^{(n)})/2$ ($n \geq 0$), and by using $\varphi^{(1)} = \varphi^{(0)} = v^{(1)}$ we get

$$\|v^{(n)} - v\|_2^2 \leq \tfrac{1}{2}(\|\varphi^{(n+1)} - v\|_2^2 + \|\varphi^{(n)} - v\|_2^2) \leq \kappa^2(\delta + \varepsilon)^{2n}\|v^{(0)} - v_2^2,$$

from which the proposition follows.

REFERENCES

1. A. J. Semtner, 'History and methodology of modelling the circulation of the world ocean', in J. J. O'Brien (ed.), *Advanced Physical Oceanographic Numerical Modelling*, Reidel, Dordrecht, 1986.
2. A. J. Semtner, 'An oceanic general circulation model with bottom topography', *Numerical Simulation of Weather and Climate, Tech. Rep. 9*, Department of Meteorology, University of California, Los Angeles, CA, 1974.
3. M. D. Cox, 'A primitive equation three-dimensional model of the ocean', *GFDL Ocean Group Tech. Rep. 1*, GFDL/NOAA, Princeton University, 1984.
4. D. E. Dietrich, M. G. Marietta and P. J. Roache, 'An ocean modelling system with turbulent boundary layers and topography: numerical description', *Int. j. numer. methods fluids*, 7, 833–855 (1987).
5. P. M. Gresho and R. L. Sani, 'On pressure boundary conditions for the incompressible Navier–Stokes equations', *Int. j. numer. methods fluids*, 7, 1111–1145 (1987).
6. E. A. H. Zuur, 'The PROSPER General Circulation Model, an adapted form of the Sandia Ocean Modelling Method: a numerical description', *Int. j. numer. methods fluids*, **13**, 251–263 (1991).
7. J. Pedlosky, *Geophysical Fluid Dynamics*, Springer, New York, 1987.
8. A. E. Gill, *Atmosphere–Ocean Dynamics*, Academic, New York, 1982.
9. J. L. Lions, R. Temam and S. Wang, 'On the equation of the large-scale ocean', *Nonlinearity*, **5**, 1007–1053 (1992).
10. G. de Rham, *Variétés Différentiables*, Hermann, Paris, 1960.
11. E. Magenes and G. Stampacchia, 'I problemi al contorno per le equazioni differenziali di tipo ellittico', *Ann. Scuola Norm. Sup. Pisa*, **12**, (1958).
12. K. Arrow, L. Hurwicz and H. Uzawa, *Studies in Nonlinear Programming*, Stanford University Press, Stanford, CA, 1968.
13. R. Temam *Navier–Stokes Equations, Theory and Numerical Analysis*, North-Holland, Amsterdam, 1984.
14. R. S. Varga, *Matrix Iterative Analysis*, Prentice-Hall, Englewood Cliffs, NJ, 1962.
15. A. H. Hageman and D. M. Young, *Applied Iterative Methods*, Academic, New York, 1981.
16. A. Arakawa and V. R. Lamb, 'Computational design of the basic dynamical processes of the UCLA general circulation model', in *Methods in Computational Physics*, Vol. 17, Academic, New York, 1977, pp. 74–265.
17. R. Glowinski, J. L. Lions and R. Tremolieres, 'Analyse Numérique des Inéquations Variationnelles, Vols I and II, Dunod, Paris, 1976.
18. M. Fortin and R. Glowinski, *Augmented Lagrangian Methods: Applications to the Numerical Solutions of Boundary-Value Problems*, North-Holland/Elsevier, Amsterdam, 1983.
19. C. Cuvelier, 'Introduction to the numerical analysis of variational inequalities', *Delft University of Technology, Rep. NA-22*, 1978.
20. R. V. Madala, 'Efficient time integration schemes for atmosphere and ocean models', in D. L. Book (ed.), *Finite Difference Techniques for Vectorized Fluid Dynamics Calculations*, Springer, New York, 1981, Chap. 4.
21. W. Y. Sun, 'A forward–backward time integration scheme to treat internal gravity waves', *Mon. Weather Rev.*, **108**, 402–407 (1980).
22. H. Sollberger, 'Le Lac de Neuchâtel', *Thèse*, Faculté des Sciences, Université de Neuchâtel', 1974.
23. A. Bapst, 'Le Lac de Neuchâtel, *Thèse*, Faculté des Sciences, Université de Neuchâtel, 1987.
24. E. A. H. Zuur and D. E. Dietrich, 'The SOMS model and its application to Lake Neuchâtel', *Aquat. Sci.*, **52**, (2), 115–129 (1990).
25. V. Thunus, E. A. H. Zuur, P. Lambert, C. -H. Godet, 'A numerical simulation of transport and sedimentation of suspended particles in Lake Neuchâtel', *Ecol. Geol. Helv.*, **87** (2), (1994).
26. K. Hutter, 'Mathematische Vorhersage von Barotropen und Baroklinen Prozessen im Zürich- und Luganersee', *Vierteljahrschr. Naturf. Ges. Zürich*, **129**, 51–92, (1984).